



# Evaluation of scanning transmission X-ray microscopy at the Mn L<sub>2,3</sub>-edges as a potential probe for manganese redox state in natural silicates

Franck Bourdelle<sup>1</sup> · Emily Lloret<sup>1</sup> · Cyril Durand<sup>1</sup> · Laura Airaghi<sup>2</sup>

Received: 26 August 2020 / Accepted: 9 March 2021 / Published online: 31 March 2021  
© The Author(s), under exclusive licence to Springer-Verlag GmbH Germany, part of Springer Nature 2021

## Abstract

Determining the Mn valence variation at the nanometer scale will be an important advance in the study of heterogeneous natural silicates. Here, the potential of the scanning transmission X-ray microscopy at the Mn L<sub>2,3</sub>-edges (640–655 eV) as a probe for manganese redox state is evaluated. For this purpose, several natural Mn-silicates (rhodonite, ardenneite, piemontite, Mn<sup>4+</sup>-silicate, jacobsonite) were analysed to identify the spectral parameters most sensitive to the Mn valence, regardless of the coordination environment, the crystal field strength, the nature and the length of the metal–ligand bonds, and the intra-atomic Coulomb and spin–orbit interactions. Two suitable spectral empirical calibrations are thus proposed, linking the Mn valence to two peak intensity ratios: one ratio of intensities from two energy points of the L<sub>2</sub> peak (at 651.7 and 655.2 eV), and one ratio of intensities from one energy point of the L<sub>2</sub> peak (at 655.2 eV) and one of the L<sub>3</sub> peak (at 641.6 eV). Thank to them, the first quantitative Mn valence maps are constructed, with a high spatial resolution (<40 nm pixel size), opening the way to exhaustive crystallochemical studies of silicates containing Mn with different valences.

**Keywords** Manganese valence · STXM · XANES spectroscopy · L<sub>2,3</sub>-edges · Redox mapping · Silicates

## Introduction

Constraining redox conditions during sediment deposition, rock formation or mineralogical transformation is of primary importance to understand the P–T–X history (pressure–temperature–composition) of geological systems. Redox conditions are usually assessed by the analysis of minerals since they partly influence their chemical composition. The evaluation of redox conditions is often based on the iron redox state, i.e. by the quantification of the Fe<sup>3+</sup>/Fe<sup>2+</sup> ratio in minerals—mainly silicates, major constituents of crusts—when they can contain both divalent and trivalent cations (i.e. Inoue et al. 2018). More rarely, the redox state of other metals is investigated, as manganese.

However, Mn—which can be present as Mn<sup>2+</sup>, Mn<sup>3+</sup> and sometimes-but-rarely Mn<sup>4+</sup>—could be a good indicator of paleo-conditions of the rock formation (Loomer et al. 2007), even if Mn-silicates, specially P–T–X sensitive silicate solid solution such as phyllosilicates, are infrequent, at the very least not ubiquitous in sedimentary and metamorphic rocks, and that the Mn content of these silicates is low. In this way, Sussenberger et al. (2018) suggest that Mn content in chlorite could be a proxy for chemo-stratigraphic conditions in a depositional environment. For their part, Bobos et al. (2018) establish a link between Mn-chlorite and wolframite, the Mn content in chlorite becoming an indicator of W–Mo mineralisation.

Unfortunately, authors could not determine the Mn<sup>3+</sup>/Mn<sup>2+</sup> ratio which would have noticeably modified the chlorite structural formula calculation, and potentially the subsequent interpretations. In the past, different techniques have been envisaged for this purpose, including electron microprobe analysis (EMPA, e.g. Albee and Chodos 1970), X-ray photoelectron spectroscopy (XPS, e.g., Ilton et al. 2016) or X-ray absorption near edge structure (XANES) spectroscopy at the K-edge (e.g. Manceau and Gallup 2005; Manceau et al. 2012). However, none of these methods provides a

✉ Franck Bourdelle  
franck.bourdelle@univ-lille.fr

<sup>1</sup> Univ. Lille, Institut Mines-Télécom, Univ. Artois, Junia, ULR 4515 - LGCgE, Laboratoire de Génie Civil et géo-Environnement, 59000 Lille, France

<sup>2</sup> University of Orléans, CNRS, BRGM, ISTO, UMR 7327, 45071 Orleans, France

nanometer-scale spatial resolution, which could be particularly useful to identify chemical and redox zonation patterns in low-temperature crystals (e.g. Bourdelle et al. 2018). On the other hand, several studies (e.g., Garvie and Craven 1994; van Aken and Liebscher 2002) have shown that electron energy-loss spectroscopy (EELS) carried out in a transmission electron microscope (TEM) is a powerful method for determining the redox state of transition metals at a submicrometric resolution, including Mn in silicates, but sometimes induces severe beam damage effects, such as electron beam-induced reduction of manganese (Lauterbach et al. 2000; de Groot et al. 2010; Livi et al. 2012). The XANES spectroscopy at the  $L_{2,3}$ -edges is often proposed as a powerful alternative and is increasingly used in the Earth sciences. First, the X-ray energies required for XANES analysis are lower at the  $L_{2,3}$ -edges (between ~640 and 655 eV) than at the K-edge (between ~6500 and 6580 eV), allowing higher resolutions, i.e. < 0.1 eV and ~30 nm at existing synchrotron facilities. Second, the X-ray incident beam is less destructive for samples than the TEM-EELS electron beam.

The XANES spectroscopy at the  $L_{2,3}$ -edges is based on the  $2p \rightarrow 3d$  electronic transition, which is sensitive to—among other parameters—the metal valence (e.g. Garvie and Craven 1994). de Groot (1994) describing in detail the complex physical basis of Mn  $L_{2,3}$ -edges, underlined that Mn valence can be obtained from  $L_{2,3}$ -edge spectra by a multiplet calculation. However, this approach remains difficult to use in the case of natural minerals whose structure has not been beforehand determined. Otherwise, the Mn valence can be evaluated by fitting  $L_{2,3}$ -edge spectra with a combination of reference spectra, but this requires  $Mn^{2+}$ ,  $Mn^{3+}$ ,  $Mn^{4+}$  reference compounds, with Mn in the same local coordination environment than the studied sample. Consequently, several authors have turned to empirical approaches, trying to find a spectral parameter depending only (or at least, mainly) on the Mn valence. The white-line ratio, calibrated by van Aken and Liebscher (2002), is probably the best known, linking the formal transition metal valence to the ratio of integral intensity (over a 2 eV window) of the  $L_3$  and  $L_2$  excitation peaks. Recently, Wang et al. (2018) used the integrated L-edge intensity, considering it is proportional to the total number of  $3d$  holes localized in the X-ray absorber (normalized to this invariant edge jump), while Risch et al. (2017) proposed a linear correlation between Mn valence and the energy of the center of gravity of the Mn  $L_3$ -edge peak. But these methods, a review of which was proposed by Tan et al. (2012), were often calibrated for Mn-oxides but were not tested on Mn-silicates, which present specific structures.

Moreover, synchrotron facilities make it possible to carry out Mn  $L_{2,3}$ -edge XANES spectroscopy with a scanning transmission X-ray microscope (STXM), one spectrum being one image pixel of the studied sample area (e.g. Bourdelle et al. 2013). This makes it possible to consider

extracting quantitative maps of Mn valence over the entire area of interest, very useful for heterogeneous natural samples containing mixed oxidation state Mn species. Pecher et al. (2003) explore the feasibility of such maps extracted from STXM-XANES data, in order to characterize the Mn charge state distribution in biominerals. Unfortunately, in absence of empirical calibration based on a spectral intensity ratio rather than an integrated area or a center of gravity calculation, the resulting maps remain qualitative.

From these observations, we want to evaluate the potential of the scanning transmission X-ray microscopy at the Mn  $L_{2,3}$ -edges as a probe for manganese redox state investigations in natural silicates, defining a suitable spectral empirical calibration allowing to construct of quantitative Mn valence maps with a high spatial resolution (nanoscale).

## Materials and methods

### Natural samples

Samples used in this study were natural silicates, containing various Mn amount and covering the three common Mn redox state (2+, 3+, 4+). As the shape of the Mn  $L_{2,3}$ -edge spectra can be influenced by, among others parameters, the Mn coordination, one oxide presenting Mn in tetrahedral coordination sites is also considered. Particles transparent to soft X-rays are needed to measure XANES spectra in the transmission mode of STXM, therefore samples are prepared as grounded powders dispersing in ethanol; a drop of which is placed (then evaporated) on a carbon holey support film placed on a 200 mesh copper grid.

The selected silicates are rhodonite, ardenite, piemontite and a  $Mn^{4+}$ -silicate (Table 1), for which chemical composition has been verified by Energy-dispersive X-ray spectroscopy, the EDX probe being coupled to a Scanning electron microscopy (QUANTA 200 SEM instrument operating at 15 kV with a 1.5 nA current; mineral standards used for EDX probe calibration: albite, diopside, orthoclase, garnet and  $MnTiO_3$ ; ZAF correction applied). Rhodonite is a  $Mn^{2+}$  pyroxenoid, where Mn is mainly in 6 coordination, sometimes in 7 (Smyth and Bish 1988; Nelson and Griffen 2005). Mn is therefore in distorted octahedral sites, defined by Mn–O bonds. The rhodonite sample used here, whose formula is  $Ca_{0.15}Mn_{0.85}SiO_3$ , comes from Gambaseta (Liguria, Italia). Ardenite is a  $Mn^{2+}$  sorosilicate described by the following formula:  $Mn_4Al_4(AlMg)(AsO_4)(SiO_4)_2(Si_3O_{10})(OH)_6$ . In it, Mn is located in a large polyhedron, based on 5 coordination via Mn–O bonds, and 2 additional coordination via Mn–OH bonds (Donnay and Allmann 1968). Here, one specimen of Ardenite-(As) from Salm-Château (Ardennes, Belgium) was studied; the composition does not present an excess of Mn (< 4 atoms per formula unit), all Mn is

**Table 1** Samples used for STXM-XANES Mn L<sub>2,3</sub>-edge investigations to Mn mean valence quantification

Type	Sample	Location	Mn valence	Position of major peaks (eV)	
				L <sub>3</sub>	L <sub>2</sub>
Silicate	Rhodonite	Gambaseta (Liguria, Italia)	2+	641.6	654.1
Silicate	Ardennite-(As)	Salm-Château (Ardennes, Belgium)	2+	641.6	654.1
Silicate	Piemontite	Prabornaz mine (Aosta, Italia)	3+	643.2	654.4
Silicate	Mn <sup>4+</sup> -silicate	Eveslogchorr (Murmansk Oblast, Russia)	4+	644.6	655.2
Oxide	Jacobsite	Langban (Filipstad, Sweden)	2+	641.6	654.1

consequently assumed as Mn<sup>2+</sup> (Nagashima and Armbruster 2010). Piemontite is a Mn-rich epidote, where Mn is in trivalent form and occupies octahedral sites. The selected specimen comes from the Prabornaz mine (Aosta, Italia), with the verified chemical formula Ca<sub>2.05</sub>(Al<sub>1.68</sub>Fe<sup>3+</sup><sub>0.49</sub>Mn<sup>3+</sup><sub>0.83</sub>)(Si<sub>2.0</sub>O<sub>7</sub>)(Si<sub>1.0</sub>O<sub>4</sub>)O(OH). The last studied Mn-silicate, a rare type of silicates that contains tetravalent Mn similarly to stavelotite-(La), was sampled at Eveslogchorr (Murmansk Oblast, Russia) combined with pectolite and has the determined empirical formula: Na<sub>0.3</sub>Ca<sub>1.4</sub>Fe<sup>3+</sup><sub>0.3</sub>Mn<sup>4+</sup><sub>5</sub>SiO<sub>14</sub>. A jacobsite sample, from Langban, (Filipstad, Sweden), was also analysed. Jacobsite is an Mn<sup>2+</sup> oxide belonging to the spinel group, with the common formula MnFe<sub>2</sub>O<sub>4</sub>. As a “normal spinel”, Mn<sup>2+</sup> occupies tetrahedral sites formed by 4 oxygens (Bosi et al. 2019).

### STXM and XANES spectroscopy

The STXM is able to record the transmitted soft X-ray intensity on each point of the pluri-micrometric-sized area of interest for each defined energy. Therefore, STXM gives 2D images for which each pixel represents a soft X-ray absorption spectrum. This is of great interest for mapping metal oxidation state variation into small crystallites (e.g. Bourdelle et al. 2013). In the present study, STXM analyses were acquired on the PolLux beamline at the Swiss Light Source (SLS, Villigen, Switzerland). The characteristics of the beamline are detailed by Raabe et al. (2008); the beam was in circular-polarisation configuration to avoid crystal lattice orientation dependency of analysis (see below). The scanning transmission X-ray microspectroscopy endstation allows to achieve stacks and linescans, i.e. a spectral map of an area and a sum of spectra for each pixel of a line, respectively. Stacks were recorded over the 635–660 eV energy range (Mn L<sub>2,3</sub>-edges) using a 0.2 eV spectral resolution and a 40 nm spatial resolution. Linescans were recorded over the same energy range, using a 0.1 eV spectral resolution. The dwell time per image- and energy- point was between 1 and 10 ms. Focus was checked

systematically for each particle. STXM-XANES data were post-processed using the aXis2000 software (Hitchcock 2012). Beam damages caused by the incident beam were assessed by monitoring spectral changes at the Mn L<sub>2,3</sub>-edges with increasing dwell times up to 20 ms.

### Spectrum processing

Spectra were extracted from stacks and linescans in form of optical density spectra (noted OD), obtained as OD =  $-\ln(I/I_0)$ , where  $I$  is the X-ray intensity transmitted from the sample, and  $I_0$  is those recorded without samples. Then two steps of processing were applied on spectra:

- (i) a linear background correction was applied to remove the contribution of lower energy absorption edges so that the pre-edge region is set to 0 optical density.
- (ii) the two edge steps resulting from transitions to unoccupied states in the continuum were subtracted using a double arctan function (Chen et al. 1995; van Aken and Liebscher 2002; Brotton et al. 2007) as:

$$f(\Delta E) = \frac{h_1}{\pi} \left( \tan^{-1} \left[ \frac{\pi}{w_1} (\Delta E - E_1) \right] + \frac{\pi}{2} \right) + \frac{h_2}{\pi} \left( \tan^{-1} \left[ \frac{\pi}{w_2} (\Delta E - E_2) \right] + \frac{\pi}{2} \right) \quad (1)$$

where  $h_1$  and  $h_2$  are the step heights of the two arctan functions,  $w_1$  and  $w_2$  are fixed peak widths and  $E_1$  and  $E_2$  are the positions of the inflection points resulting in an energy near the edge onset. Brotton et al. (2007) proposed setting the function slope  $w$  at 5 eV, to account for the slow onset of the continuum. Following this recommendation,  $w_1$  and  $w_2$  were fixed to 5 eV. For each sample, four or five spectra on different particles were extracted to evaluate the spectral variability. A total of 23 spectra were thus used in this study.

## Results and discussion

### Influences of Mn redox state, coordination and atomic environment on the shape of Mn L<sub>2,3</sub>-edge XANES spectrum

X-ray absorption near-edge structure spectra at the Mn L<sub>2,3</sub>-edges for Mn-silicates and jacobsonite are shown in Figure 1, where peaks are identified by letters (from L<sub>3</sub>-a to L<sub>3</sub>-h and from L<sub>2</sub>-a to L<sub>2</sub>-e) and linear background is subtracted. These spectra result from transitions from 2*p* core electrons to 3*d* state, 4*s* state or continuum as follows:

- two strong absorption peaks, usually noted L<sub>3</sub> and L<sub>2</sub>, due to the spin-orbit splitting of 2*p* level (van Aken and Liebscher 2002; Nishida et al. 2013) involving transitions from 2*p*<sub>3/2</sub> and 2*p*<sub>1/2</sub> states to empty 3*d* atomic orbitals, respectively. From a 2*p*<sup>6</sup>3*d*<sup>*n*</sup> ground state, the absorption process leads to a core-excited 2*p*<sup>5</sup>3*d*<sup>*n*+1</sup> final state, as 3*d*<sup>5</sup> for Mn<sup>2+</sup>, 3*d*<sup>4</sup> for Mn<sup>3+</sup> and 3*d*<sup>3</sup> for Mn<sup>4+</sup>, implying variations in absorption energy.
- edge jump steps at the bottom of L<sub>3</sub> and L<sub>2</sub> peaks, corresponding to 2*p* → continuum transitions.
- negligible contributions of 2*p* → 4*s* transitions, which are 20 times weaker in intensity than 2*p* → 3*d* transitions.

Each L<sub>3</sub> and L<sub>2</sub> peak consists of one major peak accompanied on both sides by several minor peaks. The energy position of these major peaks mainly depends (but not only) on the core-excited final state, i.e. Mn redox state: 641.6 and 654.1 eV for Mn<sup>2+</sup> (L<sub>3</sub>-b and L<sub>2</sub>-c, respectively; rhodonite, ardenite, jacobsonite), 643.2 and 654.4 eV for Mn<sup>3+</sup> (L<sub>3</sub>-e and L<sub>2</sub>-d, respectively; piemontite), 644.6 and 655.2 eV for Mn<sup>4+</sup> (L<sub>3</sub>-f and L<sub>2</sub>-e, respectively; Mn<sup>4+</sup>-silicate). In this way, spectra are qualitatively similar to those described in several previous studies, obtained using different analytical techniques (e.g. Garvie and Craven 1994; Morales et al. 2004; Zhang et al. 2010; Kubin et al. 2018).

Minor peaks arise from factors other than redox as their number, intensity and shape vary from one sample to another. Therefore, Mn<sup>2+</sup> spectra present 3 minor peaks (L<sub>3</sub>-a, L<sub>3</sub>-d and L<sub>3</sub>-g with a shoulder peak noted L<sub>3</sub>-h) around L<sub>3</sub>-b, and 2 minor peaks (L<sub>2</sub>-a, L<sub>2</sub>-b) before L<sub>2</sub>-c, more intensive (related to the intensity of major peaks) for rhodonite than for ardenite.

Mn<sup>3+</sup> and Mn<sup>4+</sup> spectra have fewer minor peaks: only two, at the same (or very close) energy position than the L<sub>3</sub> and L<sub>2</sub> Mn<sup>2+</sup> major peaks, and one more at 642.3 eV (L<sub>3</sub>-c) only for Mn<sup>4+</sup> spectra. These minor peaks are also observed in previous studies (e.g. de Groot et al. 2010; Cuartero et al. 2016; Risch et al. 2017), especially on

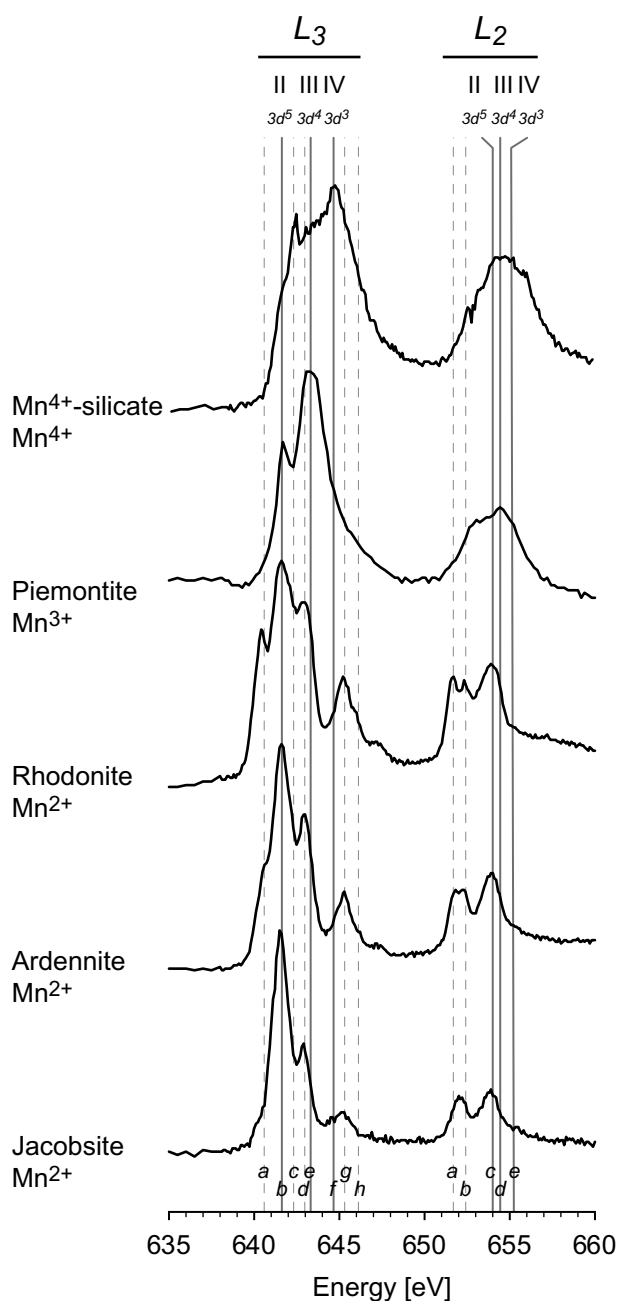


**Fig. 1** Representative XANES spectra at the Mn L<sub>2,3</sub>-edges for the Mn-silicates and jacobsonite. The spectra have been normalised to the major L<sub>3</sub> peak intensity, and some of the spectra have been shifted vertically for clarity (normalised intensity with arbitrary units). The vertical lines indicate major peaks (solid lines) and minor peaks (dashed lines). Each peak is indexed, redox states and core-excited final state configurations are mentioned

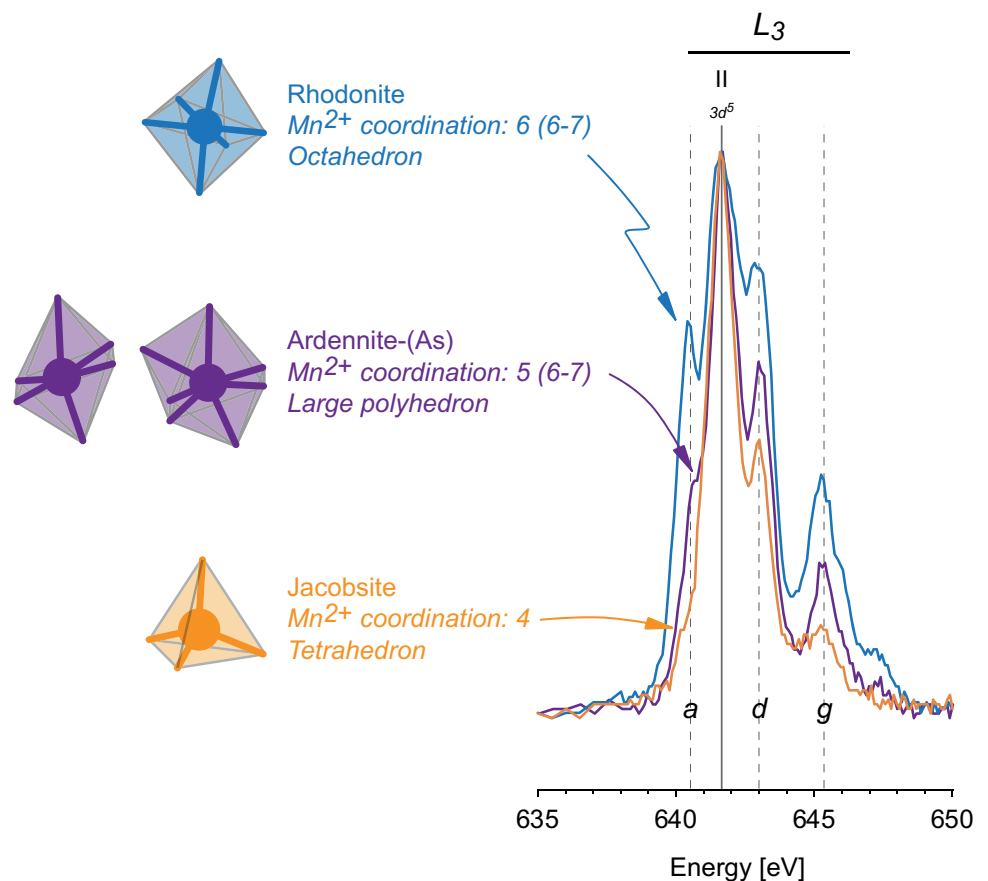
Mn-oxide spectra, and are influenced by the Mn valence and coordination environment, the crystal field strength, the nature and the length of the metal–ligand bonds, and the intra-atomic 3*d*-3*d* and 2*p*-3*d* Coulomb and spin–orbit interactions in the 2*p* core and 3*d* orbitals.

Here, no complex calculations or multiplet analyses were used to describe spectrum shape in detail as the aim of the present study is to propose an easy-to-use approach to empirically map the Mn valence in silicates. However, some comments can be made to explain (i) the general shape of the Mn-silicate spectra and (ii) the great similarity of them with Mn-oxide spectra.

In fact,  $3d$  orbitals consist of five  $d$  orbitals, as three have lobes between  $x, y, z$ -axis (noted  $d_{xy}, d_{xz}, d_{yz}$ ) and two have lobes on the axes (noted  $d_{z^2}$  and  $d_{x^2-y^2}$ ). In octahedral coordination site, the 6 ligands approach Mn along the axes, increasing by electrostatic repulsion the energy of  $d_{z^2}$  and  $d_{x^2-y^2}$  orbitals (called  $e_g$ ). Conversely,  $d_{xy}, d_{xz}, d_{yz}$  orbitals (called  $t_{2g}$ ) point between the ligands, that lowered their energies. This difference of energy between  $e_g$  and  $t_{2g}$  orbital groups defines the crystal field strength ( $\Delta_o$  or  $10 Dq$ ) (Burns 1993). In the case of 6 coordinated  $Mn^{2+}$ , the  $t_{2g}$  spectral contribution is often assigned to the  $L_3$ -a minor peak, while  $e_g$  is associated to the  $L_3$ -b major peak (Garvie and Craven 1994; de Groot 1994),  $10 Dq$  can be deducing from the energy distance between these two peaks. In Figure 2, focused on the  $L_3$ -edge part of  $Mn^{2+}$  absorption spectra (edge jump steps were subtracted), the energy gap between  $L_3$ -a and  $L_3$ -b is very weak ( $<1$  eV), suggesting a low  $10 Dq$  value. The comparison with  $10 Dq$

calculations and estimates from experiments previously published (Garvie and Craven 1994; Garvie et al. 1994; Pérez-Dieste et al. 2004) confirms that  $10 Dq$  value is probably around 0.5 or 1 eV. The energy difference between  $t_{2g}$  and  $e_g$  orbital groups remains, therefore, weak enough for Mn to be in high-spin state (Burns 1993), which is the most common spin configuration for Mn (Garvie and Craven 1994; de Groot 1994). Figure 2 also shows that the energy position of  $L_3$ -a is always the same whatever the  $Mn^{2+}$  mineral studied in our conditions, but that its intensity (related to  $L_3$ -b major peak intensity) is variable. This observation is also suitable for other minor peaks  $L_3$ -d and  $L_3$ -g, suggesting the contribution of another significant factors. In fact,  $Mn^{2+}$  in rhodonite, ardenite and jacobsite is located in different coordination sites, with different Mn-ligand bond length and different type of ligands. In rhodonite,  $Mn^{2+}$  occupies octahedral sites slightly distorted, elongated, due to the global structure, linked to 6 O (Smyth and Bish 1988). This configuration leads to an energy splitting between  $d_{x^2-y^2}$  and  $d_{z^2}$  orbitals ( $E_{d_{x^2-y^2}} > E_{d_{z^2}}$ ) on the one hand, and between  $d_{xy}$  and  $d_{xz}, d_{yz}$  orbitals ( $E_{d_{xy}} > E_{d_{xz}}$  and  $E_{d_{yz}}$ ) on the other hand. In ardenite,  $Mn^{2+}$  is located in a large polyhedron with a 6 or 7 coordination configuration, with O and OH as ligands (Donnay and Allmann 1968), also implying a substantial change in orbital energies. In jacobsite,  $Mn^{2+}$  is surrounded

**Fig. 2** Focus on  $L_3$ -edge for  $Mn^{2+}$  phases (rhodonite, ardenite, jacobsite). The spectra have been normalised to the major  $L_3$  peak intensity. Coordination (number of O ligands and sites) is specified for each phase





by 4 O in a tetrahedral site. But in this case, the 4 ligands are closer to the  $d_{xy}$ ,  $d_{xz}$ ,  $d_{yz}$  orbitals ( $t_2$ ) than to the  $d_{z^2}$ ,  $d_{x^2-y^2}$  orbitals ( $e$ ), leading to an inversion of the splitting energy,  $t_2$  orbital group having higher energy than  $e$  orbital group (Burns 1993). Differences in spectrum shapes, especially the intensities of  $t_{2g}$  or  $t_g - L_3$ -a (virtually disappeared in the case of jacobsite),  $L_3$ -d and  $L_3$ -g peaks, must be related to the coordination and the ligands of Mn. From an empirical point of view, the intensity of minor peaks decreases proportionally to the number of Mn–O bonds. On the other hand, the similarity of Mn-silicate (i.e.  $Mn^{2+}$ ,  $Mn^{3+}$  and  $Mn^{4+}$ -silicates) and Mn-oxide spectra (from this study and literature) tends to indicate that, as a first approximation, the extended atomic environment (i.e. beyond the coordination site receiving Mn) has negligible influence compared to that of the near coordination.

Consequently, an empirical calibration linking a spectral parameter to the Mn mean valence must be mainly based on major peaks, most sensitive to redox, without taking into account an energy window (as white line ratio method) that might include minor peaks, most sensitive to the Mn coordination and the surrounding atomic environment. An empirical calibration is possible especially since the 10 Dq is weak (van der Laan and Kirkman 1992).

### Mn redox state estimation from $L_{2,3}$ -edge XANES spectra

As three valence states of Mn could be present in silicates, it is not possible to determine easily, directly and empirically the relative proportion of each of them. As an alternative, XANES spectra allow to assess the Mn mean valence which, coupled to a structural formula obtained with an independent method, gives a strong indication of the likely  $xMn^{2+} + yMn^{3+} + zMn^{4+}$  combination.

As referenced in Fig. 1, the main variation in the XANES spectra of silicates with the Mn valence involves the energy position of the  $L_3$  major peak. More precisely, the  $L_3$  major peak shifts to higher energies with increasing Mn charge, by a step of 1.4–1.6 eV. However, because this step and Mn valence are not linearly linked, Risch et al. (2017) prefer to use the center of gravity of the  $L_3$ -edge peak. From Mn-oxides, authors propose a linear correlation implying to take in consideration the  $L_3$  minor peaks in addition to major peaks. A such correlation was established here for silicates (Fig. 3) and demonstrates the influence of minor peaks, i.e. of the type of coordination sites in which Mn occurs. Considering only the mineral phases where Mn occupies octahedral sites (piemontite, rhodonite) and  $Mn^{4+}$ -silicate, the relationship between nominal Mn valence and the  $L_3$  center of gravity is linear, with a  $R^2 = 1$ . However, taking into account the ardennite in which Mn occupies a large polyhedron or jacobsite in which Mn is in tetrahedral sites, the

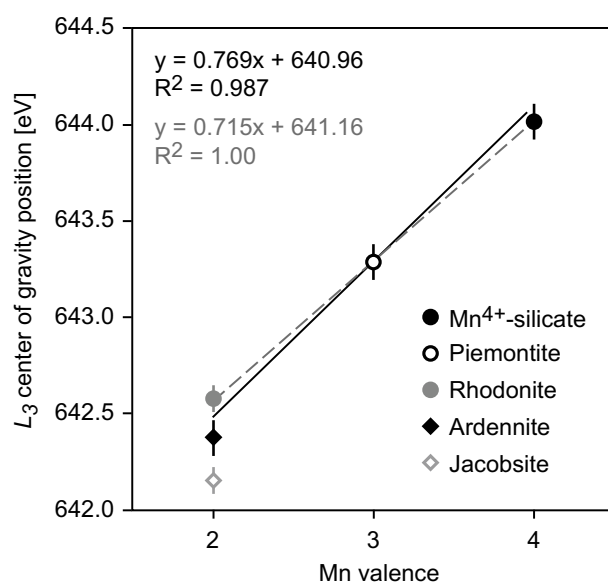


**Fig. 3**  $L_3$ -edge center of gravity from XANES spectra versus Mn valence for the selected silicates. Error bars represent the standard deviation calculated on the base of 4 or 5 spectra for each sample. Value for jacobsite is given for information, but not taken into account for calibration calculation

energy position of the  $L_3$  center of gravity for  $Mn^{2+}$  phases depends on  $L_3$ -a,  $L_3$ -d and  $L_3$ -g peak weight and not only of Mn redox state. Mainly, the  $L_3$  center of gravity is a spectral parameter including a peak area, not extractable from a stack. This approach, therefore, does not allow to easily map the Mn valence from STXM-XANES data.

To construct a redox map, it becomes therefore necessary to propose a new purely-empirical calibration of Mn valence with a simple spectral parameter, using selected energy points (and not a spectral surface as white line ratio or center of gravity), that does not need to have any physical significance (as an intensity ratio). Considering only the silicates (jacobsite is excluded) and the 13 identified peaks (Fig. 1), 78 ratios of two peak intensities can be calculated, plus their inverses, namely 156 possibilities. But only 12 peak intensity ratios are in correlation with the Mn valence with a coefficient of determination higher than 0.98. In fact, the  $R^2$  is very poor for intensity ratios implying major peaks of  $Mn^{3+}$  and minor peaks of  $Mn^{2+}$ . On the 12 peak intensity ratios correlated to Mn valence, 3 only used peaks from  $L_3$  peak, 6 only used peaks from  $L_2$  peak, and 3 used peaks from  $L_3$  and  $L_2$  peaks. Among them, we prefer those using peaks common to several valences and major peaks. Two correlations are therefore selected as calibration. The spectral parameter of the first calibration is a ratio between the intensities at two energy points of the  $L_2$ -edge, i.e. at  $L_2$ -a in  $Mn^{2+}$  spectra (651.7 eV) and at the  $L_2$ -e major peak in  $Mn^{4+}$  spectra (655.2 eV). The spectral parameter is then expressed as follows:

$$R_{L_2} = \frac{I(\text{at } 655.2 \text{ eV})}{I(\text{at } 651.7 \text{ eV})}$$

From this parameter, the first calibration equation is (Fig. 4a):

$$\text{Mn mean valence} = \frac{R_{L_2} + 6.706}{3.512} \quad (2)$$

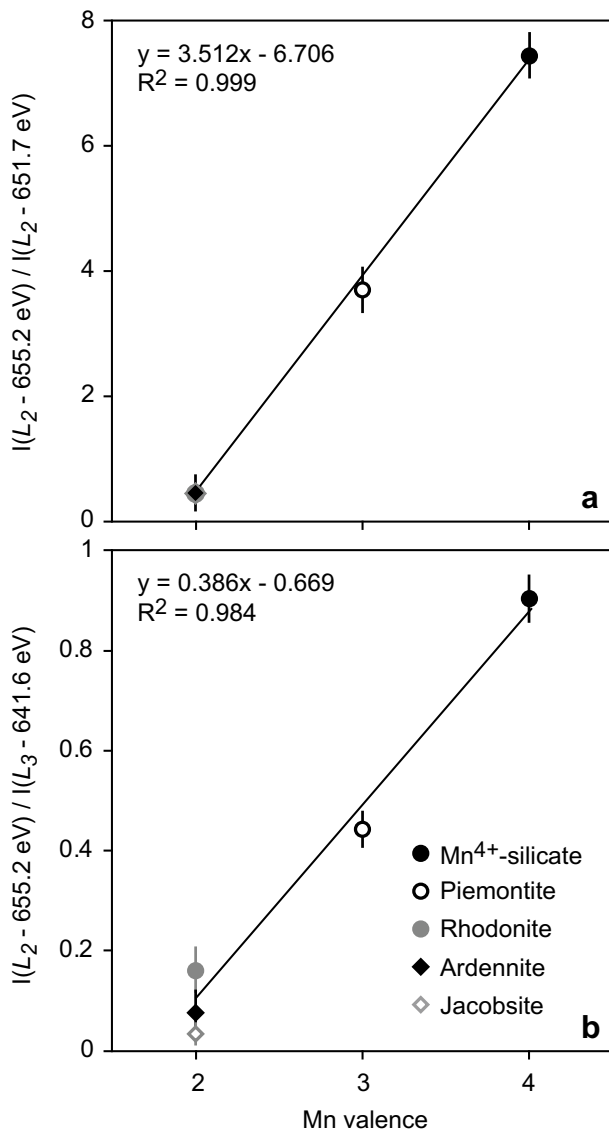


**Fig. 4**  $L_{2,3}$ -edge intensity ratios from XANES spectra versus Mn valence for the selected silicates. **a**  $R_{L_2}$  ratio, using selected intensities at two energy points (i.e. 651.7 and 655.2 eV) of the  $L_2$ -edge. **b**  $R_{L_{2,3}}$  ratio, using selected intensities at one energy point (i.e. 641.6 eV) of the  $L_3$ -edge and one energy point (i.e. 655.2 eV) of the  $L_2$ -edge. Error bars represent the standard deviation calculated on the base of 4 or 5 spectra for each sample, i.e. 18 spectra in total. Values for jacobsite are given for information, but not taken into account for calibration calculation

It shows a coefficient of determination ( $R^2$ ) of 0.999. The same  $R_{L_2}$  value is obtained for ardennite and rhodonite (and jacobsite, not used for calibration), showing that  $R_{L_2}$  is not influenced by the Mn atomic environment but only by the Mn valence. This perfect correlation can be used to map Mn valence on unknown samples since only two images (at fixed energy, i.e. 651.7 and 655.2 eV) are required.

The spectral parameter defined in the second calibration is the ratio between the intensity at  $L_3$ -edge energy point (i.e. 641.6 eV, the energy position of the  $L_3$ -b major peak of  $Mn^{2+}$  spectra) and the intensity at  $L_2$ -edge energy point (i.e. 655.2 eV, the energy position of the  $L_2$ -e major peak of  $Mn^{4+}$  spectra). The calibration equation is expressed as follows (Fig. 4b):

$$\text{Mn mean valence} = \frac{R_{L_{2,3}} + 0.669}{0.386} \quad (3)$$

with

$$R_{L_{2,3}} = \frac{I(\text{at } 655.2 \text{ eV})}{I(\text{at } 641.6 \text{ eV})}$$

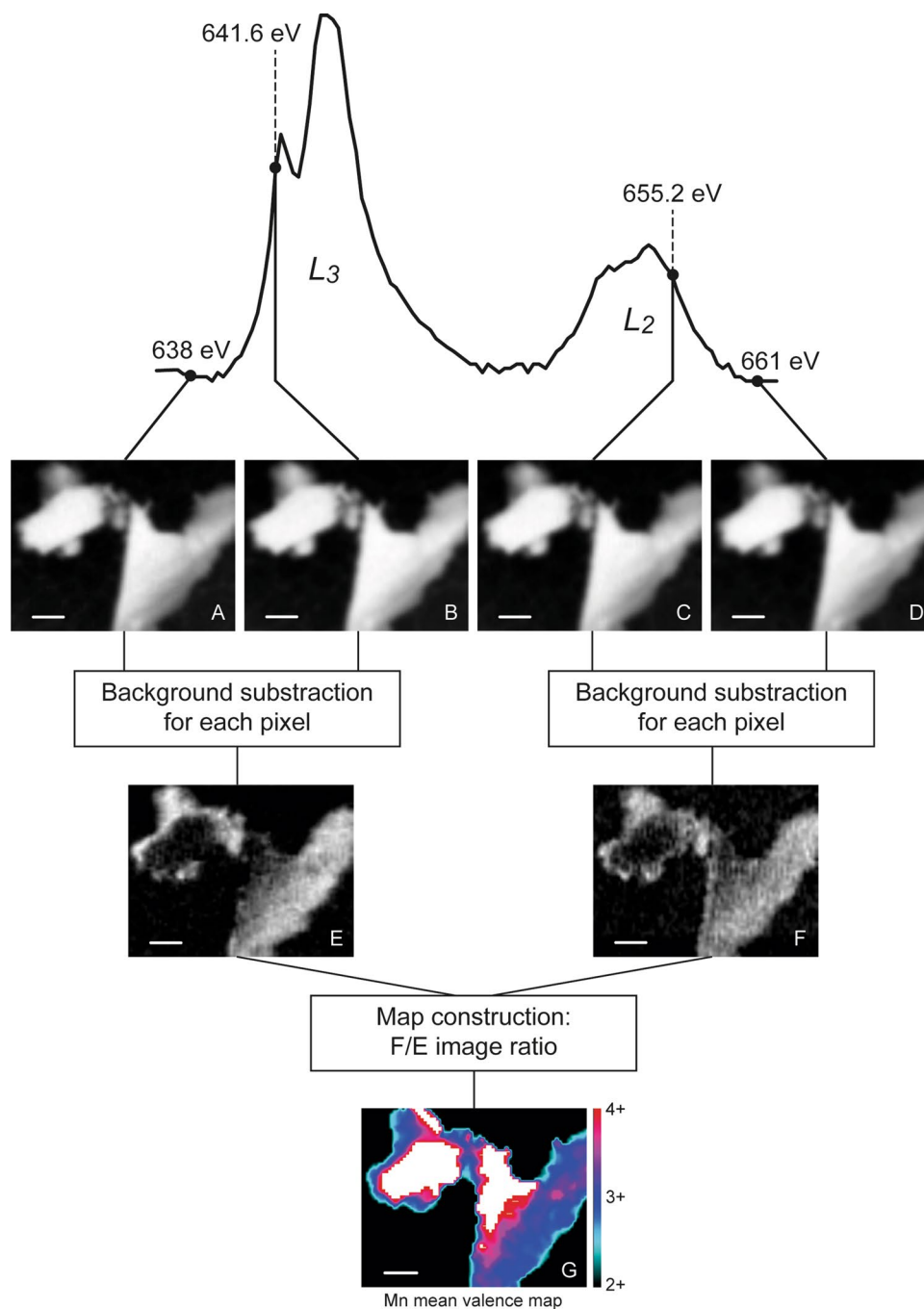
The coefficient of determination for this second calibration ( $R^2$ ) is 0.984, slightly lower than the one of the first calibration. The difference between  $R_{L_{2,3}}$  values for rhodonite and ardennite (and jacobsite) suggests a contribution of Mn atomic environment in addition to the Mn valence dependence. However, taking an intensity on the  $L_3$ -edge (which is more intense than the  $L_2$ ) and one on the  $L_2$ -edge improves the signal-to-noise ratio. As for the first correlation proposed, the construction of a Mn valence map from STXM-XANES data is made possible by Eq. (3).

### STXM-XANES coupling: Mn redox mapping

The scanning properties of the microscope allow to record a stack of 125 energy images over the 635–660 eV with a spectral resolution of 0.2 eV. Equations (2) and (3) permit the Mn mean valence to be estimated from the spectrum intensities at two energies. This gives the possibility to easily map the Mn valence from two energy images, and use one of the two calibrations proposed.

In fact, two other XANES images are required in addition to the two images used for mapping, to subtract the background at each pixel of the images. Therefore, only four energy images should be selected to calculate the  $R$  parameter. In Fig. 5, the calibration procedure that uses Eq. (3) and the  $R_{L_{2,3}}$  parameter is drawn as example (piemontite sample). It is obtained by extracting one image at 641.6 eV, one at 655.2 eV, one in the pre-edge (to apply the “linear background correction” at each pixel of the 641.6 eV image), and one beyond the energy corresponding to the  $L_2$  peak

**Fig. 5** Determination of the Mn valence from 4 selected energy images: one image in the pre-edge (to apply the “linear background correction” at each pixel of the image; image **a**), one at 641.6 eV ( $L_3$ -b major peak of  $Mn^{2+}$ ; image **b**), one at 655.2 eV ( $L_2$ -e major peak of  $Mn^{4+}$ ; image **c**) and one beyond the  $L_2$ -edge (to remove the edge step of the arctan function; image **d**). Finally, the ratio of the resulting 641.6 and 655.2 eV images (**e**, **f**) can be used to determine the  $R_{L_{2,3}}$  parameter at each pixel of the image and obtain Mn redox mapping (**g**). All images are OD images, where piemontite and no Mn-silicate are the light-grey and dark phases on image E, respectively. White scale: 1  $\mu m$



(to remove the linear background and the second edge step of the arctan function at each pixel of the 655.2 eV image). The ratio of corrected 641.6 and 655.2 eV images can then be used to determine the  $R_{L_{2,3}}$  for each pixel and to obtain the map of Mn redox state. In this way, the linear background is represented by only one energy at one energy position, so this point should be fairly close to the first peak (638 eV in Fig. 5). In the case of spectra with a strong background noise, it is possible to make an “image average” (giving an

average value of the linear pre-peak background) by selecting about 10 images between 625 and 639 eV, by adding them and then by dividing the resulting “image sum” by 10 thanks to the aXis2000 software.

If Eq. (2) is chosen for calibration, the images required to calculate the  $R_{L_2}$  parameter need to be selected at 651.7 eV ( $L_2$ -a), at 655.6 eV ( $L_2$ -e), at the inflexion point between the  $L_3$  peak and the  $L_2$  peak (to remove the background from the 651.7 eV), and one beyond the  $L_2$  peak (to remove the linear



background and the second edge step of the arctan function for each pixel of the 655.2 eV image). By applying the same procedure as before, the Mn map can be reconstructed only from the  $L_{2}$ -edge data.

Resulting quantitative Mn redox maps are a useful tool to identify the Mn mean valence of unknown nanometric particles but have some limitations. On a map built from  $R_{L_{2,3}}$  parameter for a no-pure piemontite sample constructed with Eq. (3) (Fig. 6), the Mn-free crystallites appear in white (Figs. 5g, 6) while in areas where the particle is too thick and/or highly concentrated in Mn, valence is overestimated (Fig. 6b). In the first case, the absence of Mn leads to calculate the ratio between two too weak absorption pixels (Fig. 5e,f). In the second case, too high X-ray absorption causes an absorption saturation of the  $L_{3}$  peak, which is more intense than the  $L_{2}$  peak. This phenomenon generates a nonlinear response of the absorption detection, artificially modifying the relative peak intensities and affecting the  $R_{L_{2,3}}$  calculation and overestimating the Mn valence. Although more sensitive to the signal/noise ratio, the use of the  $R_{L_2}$  parameter and Eq. (2) to map the Mn valence, based exclusively on the  $L_2$  peak, may provide a favourable way to circumvent absorption saturation issues encountered with the  $L_3$  peak (Fig. 6c).

The spatial averaging effect of the X-ray beam over the pixel size (i.e., 40 nm) must also be taking into account. This effect fixes the limit of the minimum distance over which phase contacts or phase rims can be discriminated.

Surpassing these limitations easily identifiable, the STXM-based XANES quantitative map becomes a precise tool, giving an estimate of Mn valence with a high spatial resolution, as demonstrated by the map of piemontite in Fig. 6.

### Assessment of saturation and beam damage effects

Although EELS is known to cause more damage than STXM on the structure of minerals (e.g. de Groot et al. 2010), the latter is nonetheless a method that damages particles during analysis if precautions are not taken. Potentially, the repeated scan of particles at each energy point of a spectrum can alter the structure of the crystallites, and consequently the Mn mean valence estimate. A stack recorded on a  $5 \times 5 \mu\text{m}$  area, obtained with a spatial resolution of 50 nm, a spectral resolution of 0.2 eV and a dwell time of 5 ms per energy- and image-point results in a total analysis time of 2.5 h (dead time excluded) and of 0.875 s per image-point. To evaluate beam damages, spectral changes at the Mn  $L_{2,3}$ -edges were monitored with increasing dwell times, from 1 to 20 ms per energy- and image-point. The resulting XANES spectra do not show significant changes, while  $R_{L_2}$  and  $R_{L_{2,3}}$  parameters are only slightly affected, varying by less than 5%. Consequently, the effect of beam damages on the Mn valence

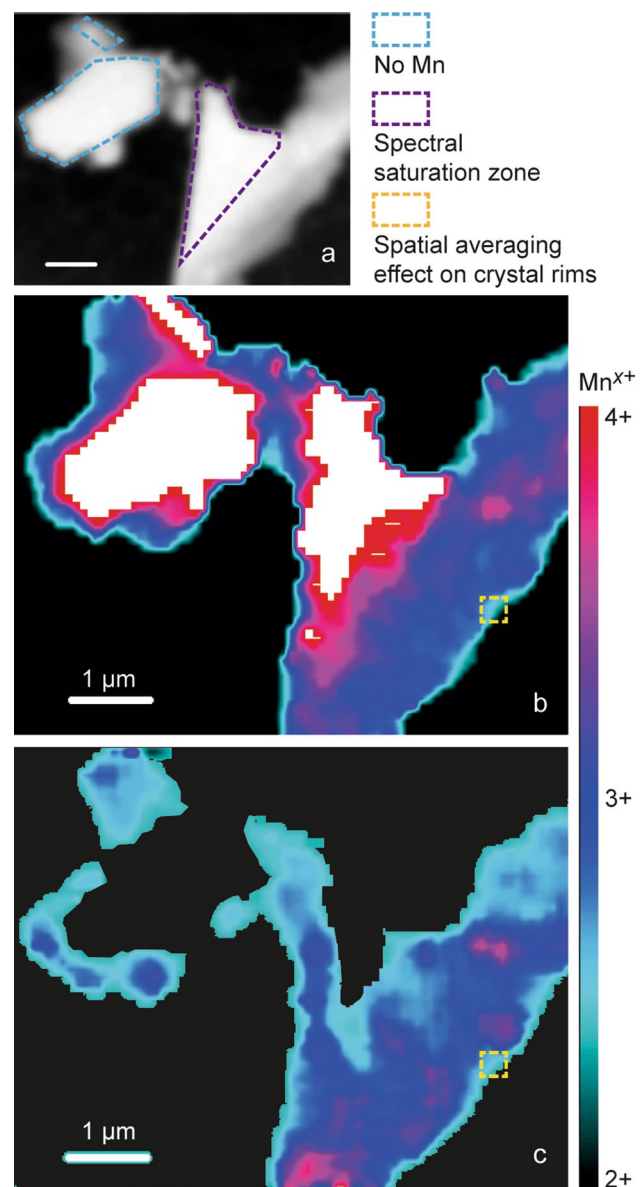


**Fig. 6** Quantitative Mn redox nanomapping on particles from no-pure piemontite sample. **a** Optical density image at 641.6 eV, where the piemontite and no-Mn silicate particles are the light-grey and white phases, respectively. **b** Manganese redox mapping, calculated from the  $R_{L_{2,3}}$  parameter coupled with the Eq. (3). **c** Manganese redox mapping, calculated from the  $R_{L_2}$  parameter coupled with Eq. (2). The spatial averaging effect of the X-ray beam over the pixel size (i.e., 40 nm) sets the limit of the minimum distance (turquoise rims, underlined by a yellow square). No-Mn silicates, identified by blue dashed polygon on the OD image, appear in white on the redox map **b** and in black for no Mn absorption on the redox map **c** and image **e** of Fig. 5. Areas where the particle thickness is too high to obtain no-saturated images (see "Assessment of saturation and beam damage effects" section)—highlighted by a purple polygon on the OD image—lead to the overestimate of Mn valence (pink and red zones of the redox map **b**), up to the total saturation (appearing in white on the map). Areas presenting no-too-thick piemontite particles (i.e. the rest of the OD image) appear in blue on the Mn redox maps, testifying of trivalent manganese

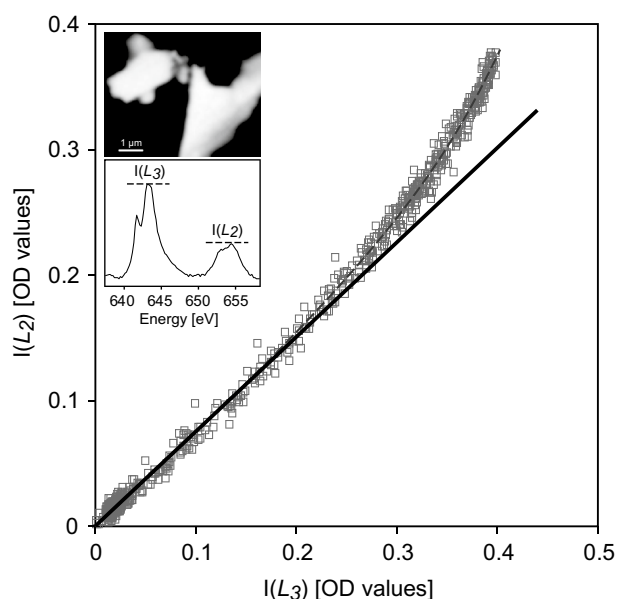


**Fig. 7** Difference, pixel by pixel, of intensity detected between the  $L_3$  major peak and the  $L_2$  major peak images (in which a pre-edge image was subtracted) for a no-pure piemontite sample (4661 pixels). The dashed line was calculated from a quadratic equation. *Insets*: representative spectra and optical density image (641.6 eV) for a no-pure piemontite sample

estimate is negligible in the typical dwell time range used during routine analyses.

The saturation of spectrum can also alter the assessment of  $R_{L_2}$  and  $R_{L_{2,3}}$  parameters (see “[STXM-XANES coupling: Mn redox mapping](#)” section). This phenomenon occurs when particles are too thick or too rich in Mn (or a combination of both), leading to a distortion of the spectrum. Hanhan et al. (2009) for Ca and Bourdelle et al. (2013) for Fe proposed to evaluate the maximum intensity of the major peak not to be exceeded to avoid saturation effect. Applying a similar approach, the maximum Mn  $L_3$  peak intensity, below which the  $L_3/L_2$  peak intensity ratio varies linearly and the spectrum is undistorted, was determined. For this, a stack was recorded on a powder of piemontite sample ( $Mn^{3+}$ ) with particles of various thicknesses. Figure 7 plots the intensity of the  $L_3$  major peak according to the one of  $L_2$  major peak for each image-point. The intensities of these two peaks increase linearly until  $\sim 0.25$  OD. When the particle is thick enough for the  $L_3$  major peak intensity to exceed 0.25 OD, the  $L_3/L_2$  intensity ratio no longer evolves linearly, i.e. the intensity of  $L_2$  major peak increases faster than that of  $L_3$  major peak, reflecting the spectra distortion for the considered image-points. This observation is also valid for  $Mn^{2+}$  and  $Mn^{4+}$  spectra. Consequently, all the quantitative data in this study were therefore obtained from areas presenting a  $L_3$  major peak intensity lower than 0.25 OD. It should be noted that

Mn is much more sensitive to saturation phenomena than Fe (saturation effects at  $> 1.5$  OD at the Fe  $L_{2,3}$ -edges; Bourdelle et al. 2013), i.e. saturation effects appear at relatively low Mn content (concentration or weak sample thickness). On an indicative basis, piemontite, which is a phase that is not very rich in Mn, presents saturated spectra for a crystallite thickness higher than  $\sim 150$  nm, while Mn-rich jacobsonite shows saturation effects on the spectrum when crystallite thickness is around 70 nm.

The crystal orientation compared with the direction of polarisation of the X-ray beam may also influence the spectrum shape. This process is called linear dichroism (Benzerrara et al. 2011) and can be thwart using a circular polarized beam as here. The residual dichroism effect was evaluated by comparing spectra from different piemontite particles with various orientations. No change in spectrum shape was observed, and the impact of particle orientation on the Mn mean valence estimate remained undetectable.

## Conclusion

In the present work, we explore the possibility to construct quantitative Mn redox maps for silicates using the STXM coupled with XANES spectroscopy at the Mn  $L_{2,3}$ -edges. With fairly limited precautions, we demonstrate that this type of maps could be obtained from two easy-to-use empirical calibrations linking the Mn mean valence to a simple ratio of intensities from selected energy positions. We applied this approach on a mix of piemontite and no-Mn phase sample, demonstrating the potential of it to assess the Mn valence at the nanoscale through micrometric areas. Even if calibrations and map construction have yet to be tested on silicates containing Mn under several oxidation states, as Mn-phyllsilicates, these results pave the way for the study of nanochemical zonations in heterogeneous silicates.

**Acknowledgements** We are most grateful to the PSI SLS synchrotron, especially Benjamin Watts (PolLux beamline) for technical advice. Thanks are extended to Philippe Recourt (LOG, Univ. Lille) for sample preparation and to Francis Coune for providing ardennite sample. The authors wish also to thank the editor and the two anonymous reviewers for comments and suggestions that improved the paper. This study was financially supported by LGCgE.

**Funding** This study was financially supported by LGCgE (laboratory funds).

**Availability of data and material** XANES spectra are available on request from [franck.bourdelle@univ-lille.fr](mailto:franck.bourdelle@univ-lille.fr).

**Code availability** Not applicable.

## Declarations

**Conflicts of interest** Not applicable.

## References

- Albee AL, Chodos AA (1970) Semiquantitative electron microscope determination of  $\text{Fe}^{2+}/\text{Fe}^{3+}$  and  $\text{Mn}^{2+}/\text{Mn}^{3+}$  in oxides and silicates and its application to petrologic problems. *Am Mineral* 55:491–501
- Benzerara K, Menguy N, Obst M, Stolarski J, Mazur M, Tyliszczak T, Brown GE Jr, Meibom A (2011) Study of the crystallographic architecture of corals at the nanoscale by scanning transmission X-ray microscopy and transmission electron microscopy. *Ultramicroscopy* 111:1268–1275
- Bobos I, Noronha F, Mateus A (2018) Fe-, Fe, Mn- and Fe, Mg-chlorite: a genetic linkage to W, (Cu, Mo) mineralization in the magmatic-hydrothermal system at Borralha, northern Portugal. *Mineral Mag* 82:S259–S279
- Bosi F, Biagioni C, Pasero M (2019) Nomenclature and classification of the spinel supergroup. *Eur J Mineral* 31:183–192
- Bourdelle F, Benzerara K, Beyssac O, Cosmidis J, Neuville DR, Brown GE, Paineau E (2013) Quantification of the ferric/ferrous iron ratio in silicates by scanning transmission X-ray microscopy at the  $\text{Fe L}_{2,3}$  edges. *Contrib Mineral Petrol* 166:423–434
- Bourdelle F, Beyssac O, Parra T, Chopin C (2018) Nanoscale chemical zoning of chlorite and implications for low-temperature thermometry: application to the Glarus Alps (Switzerland). *Lithos* 314:551–561
- Brotton SJ, Shapiro R, van der Laan G, Guo J, Glans PA, Ajello JM (2007) Valence state fossils in Proterozoic stromatolites by L-edge X-ray absorption spectroscopy. *J Geophys Res Biogeosci* 112:G3
- Burns R (1993) Mineralogical applications of crystal field theory (Cambridge Topics in Mineral Physics and Chemistry). Cambridge University Press, Cambridge. <https://doi.org/10.1017/CBO9780511524899>
- Chen CT, Idzerda YU, Lin HJ, Smith NV, Meigs G, Chaban E, Ho GH, Pellegrin E, Sette F (1995) Experimental confirmation of the X-ray magnetic circular-dichroism sum-rules for iron and cobalt. *Phys Rev Lett* 75:152–155
- Cuartero V, Lafuerza S, Rovezzi M, Garcia J, Blasco J, Subias G, Jiménez E (2016) X-ray absorption and emission spectroscopy study of Mn and Co valence and spin states in  $\text{TbMn}_{1-x}\text{Co}_x\text{O}_3$ . *Phys rev B* 94:155117
- de Groot FMF (1994) X-ray absorption and dichroism of transition metals and their compounds. *J Electron Spectros Relat Phenomena* 67:529–622
- de Groot FMF, de Smit E, van Schooneveld MM, Aramburo LR, Weckhuysen BM (2010) In-situ scanning transmission X-ray microscopy of catalytic solids and related nanomaterials. *Chem Phys Chem* 11:951–962
- Donnay G, Allmann R (1968)  $\text{Si}_3\text{O}_{10}$  groups in the crystal structure of ardenite. *Acta Cryst B* 24:845
- Garvie LAJ, Craven AJ (1994) High-resolution parallel electron energy-loss spectroscopy of Mn L<sub>2,3</sub>-edges in inorganic manganese compounds. *Phys Chem Miner* 21:191–206
- Garvie LAJ, Craven AJ, Brydson R (1994) Use of electron-energy loss near-edge fine structure in the study of minerals. *Am Mineral* 79:411–425
- Hanhan S, Smith AM, Obst M, Hitchcock AP (2009) Optimization of analysis of soft X-ray spectromicroscopy at the Ca 2p edge. *J Electron Spectros* 173:44–49
- Hitchcock AP (2012) aXis 2000 analysis of X-ray images and spectra. McMaster University, Hamilton
- Ilton ES, Post JE, Heaney PJ, Ling FT, Kerisit SN (2016) XPS determination of Mn oxidation states in Mn (hydr)oxides. *Appl Surf Sci* 366:475–485
- Inoue A, Inoue S, Utada M (2018) Application of chlorite thermometry to estimation of formation temperature and redox conditions. *Clay Miner* 53:143–158
- Kubin M, Guo M, Kroll T, Löchel H, Källman E, Baker ML, Mitzner R, Gul S, Kern J, Föhlisch A, Erko A, Bergmann U, Yachandra V, Yano J, Lundberg M, Wernet P (2018) Probing the oxidation state of transition metal complexes: a case study on how charge and spin densities determine Mn L-edge X-ray absorption energies. *Chem Sci* 9:6813
- Lauterbach S, McCammon CA, van Aken P, Langenhorst F, Seifert F (2000) Mossbauer and ELNES spectroscopy of (Mg, Fe)(Si, Al)O<sub>3</sub> perovskite: a highly oxidised component of the lower mantle. *Contrib Mineral Petrol* 138:17–26
- Livi KJT, Lafferty B, Zhu M, Zhang S, Gaillot A-C, Sparks DL (2012) Electron energy-loss safe-dose limits for manganese valence measurements in environmentally relevant manganese oxides. *Environ Sci Technol* 46:970–976
- Loomer D, Al T, Weaver L, Cogswell S (2007) Manganese valence imaging in Mn minerals at the nanoscale using STEM-EELS. *Am Mineral* 92:72–79
- Manceau A, Gallup DL (2005) Nanometer-sized divalent manganese-hydrous silicate domains in geothermal brine precipitates. *Am Mineral* 90:371–381
- Manceau A, Marcus MA, Grangeon S (2012) Determination of Mn valence states in mixed-valent manganates by XANES spectroscopy. *Am Mineral* 97:816–827
- Morales F, de Groot FMF, Glatzel P, Kleimenov E, Bluhm H, Hävecker M, Knop-Gericke A, Weckhuysen BM (2004) In Situ X-ray Absorption of Co/Mn/TiO<sub>2</sub> catalysts for Fischer-Tropsch synthesis. *J Phys Chem B* 108:16201–16207
- Nagashima M, Armbruster T (2010) Ardenite, tiragalloite and medaite: structural control of (As<sup>5+</sup>, V<sup>5+</sup>, Si<sup>4+</sup>)O<sub>4</sub> tetrahedra in silicates. *Mineral Mag* 74:55–71
- Nelson WR, Griffen DT (2005) Crystal chemistry of Zn-rich rhodonite (“fowlerite”). *Am Mineral* 90:969–983
- Nishida S, Kobayashi S, Kumamoto A, Ikeno H, Mizoguchi T, Tanaka I, Ikuhara Y, Yamamoto T (2013) Effect of local coordination of Mn on Mn-L<sub>2,3</sub> edge electron energy loss spectrum. *J Appl Phys* 114:054906
- Pecher K, McCubbery D, Kneeder E, Rothe J, Bargar J, Meigs G, Cox L, Nealson K, Tonner B (2003) Quantitative charge state analysis of manganese biominerals in aqueous suspension using Scanning Transmission X-ray Microscopy (STXM). *Geochim Cosmochim Acta* 67:1089–1098
- Pérez-Dieste V, Crain JN, Kirakosian A, McChesney JL, Arenholz E, Young AT, Denlinger JD, Ederer DL, Callcott TA, Lopez-Rivera SA, Himpel FJ (2004) Unoccupied orbitals of 3d transition metals in ZnS. *Phys Rev B* 70:085205
- Raabe J, Tzvetkov G, Flechsig U, Böge M, Jaggi A, Sarafimov B, Vernooij MGC, Huthwelker T, Ade H, Kilcoyne D, Tyliszczak T, Fink RH, Quitmann C (2008) PoLux: a new facility for soft X-ray spectromicroscopy at the Swiss Light Source. *Rev Sci Instrum* 79
- Risch M, Stoerzinger KA, Han B, Regier TZ, Peak D, Sayed SY, Wei C, Xu Z, Shao-Horn Y (2017) Redox processes of manganese oxide in catalyzing oxygen evolution and reduction: an in situ soft X-ray absorption spectroscopy study. *J Phys Chem C* 121:17682–17692
- Smyth JR, Bish DL (1988) Crystal structures and cation sites of the rock-forming minerals London and Boston (Unwin-Hyman Ltd.). *Mineral Mag* 52:733–734

- Sussenberger A, Pospiech S, Schmidt ST (2018) [MnO vertical bar SiO<sub>2</sub>, Al<sub>2</sub>O<sub>3</sub>, FeO, MgO] balanced log-ratio in chlorites: a tool for chemo-stratigraphic mapping and proxy for the depositional environment. 16th International Clay Conference (ICC) Location: Granada. *Clay miner* 53:351–375
- Tan H, Verbeeck J, Abakumov A, van Tendeloo G (2012) Oxidation state and chemical shift investigation in transition metal oxides by EELS. *Ultramicroscopy* 116:24–33
- van Aken PA, Liebscher B (2002) Quantification of ferrous/ferric ratios in minerals: new evaluation schemes of Fe L-23 electron energy-loss near-edge spectra. *Phys Chem Miner* 29:188–200
- Van der Laan G, Kirkman IW (1992) The 2p absorption spectra of 3d transition metal compounds in tetrahedral and octahedral symmetry. *J Phys: Condens Matter* 4:4189–4204
- Wang H, Friedrich S, Li L, Mao Z, Ge P, Balasubramanian M, Patil DS (2018) L-edge sum rule analysis on 3d transition metal sites: from d10 to d0 and towards application to extremely dilute metallo-enzymes. *Phys Chem Chem Phys* 20:8166–8176
- Zhang S, Livi KJT, Gaillot A-C, Stone AT, Veblen DR (2010) Determination of manganese valence states in (Mn<sup>3+</sup>, Mn<sup>4+</sup>) minerals by electron energy-loss spectroscopy. *Am Mineral* 95:1741–1746

**Publisher's Note** Springer Nature remains neutral with regard to jurisdictional claims in published maps and institutional affiliations.